Improvement of waste heat recuperation on an industrial textile dryer: redesign of heat exchangers network and components

Daniele Fiaschi[1], GiampaoloManfrida[1], Luigi Russo[2], Lorenzo Talluri[1]*

[1]Dipartimento di Ingegneria Industriale, University of Florence, Viale Morgagni 44, 50135 - Florence, Italy

[2]Gesco S.p.A., Z. I. Belvedere n. 83 - Ingr. 2, 53034 – Colle di Val d'Elsa (SI)

* Corresponding author. Email: daniele.fiaschi@unifi.it; Tel. +39 055 2758680

Abstract

The improvement of low temperature exhausts heat recovery network of an industrial textile – drying machine (*Stenter*/*Rameuse*) is presented.

A complete redesign of the layout of the water – gas heat exchangers network was done. The network was improved changing the original serial configuration of the heat recovery cells to a system with parallel manifolds for the water circuit. The heat transfer layout and the related heat exchangers were modelled with a dedicated thermal design code. The limited heat transfer coefficient of the internal gas side in the original configuration was improved with a "twin barrel" solution, with water in the outer annulus and exhaust gas in the inner duct equipped with internal longitudinal fins, an effective solution allowing easy fabrication and cleaning.

A second step refinement design of the heat exchangers modules, realized with an OpenFOAM® CFD procedure, allowed the final definition and optimization of the fins size and layout, which were not continuous on the whole length of the module, but staggered on the inner side and shortened to about 1/3 of the length.

Compared to the original version, the new heat exchangers network and the improved thermal design allowed an increase of the heat recovery from the exhausts of about 180%. The adoption of three staggered and segmented fins led to an increase of 97% with respect to the bare pipe.

Finally, the results of the models were validated on a test bench reproducing one full-scale section of the drying machine: the tests gave positive issues, confirming the model predictions and the correct operability of the unit. Particularly, the accuracy of prediction of water temperature was very good (less than 0.5°C difference between simulation and measurements).

Keywords:

Heat recovery, Textile dryer, Finned heat exchangers, CFD, Heat exchanger tests

33 **Nomenclature**

Symbols

A	Surface area [m^2]
C	Heat capacity [kJ/K]
Cp	Specific heat [kJ/(kg K)]
D	Diameter [m]
DP	Pressure loss [Pa]
e	Roughness [m]
h	Fluid/metal heat transfer coefficient [W/(m^2K)]
H	Height [m]
k	Conductivity [W/(mK)]
L	Length [m]
LMTD	Logarithm Mean Temperature Difference [K]
LP	Power loss [W]
m	Mass flowrate [kg/s]
N	Number [ ]
Nu	Nusselt Number
NTU	Number of Thermal Units [ ]
Pr	Prandtl Number [ ]
Ptc	Pitch [m]
Q	Heat Power [kW]
r	Radius [m]
Re	Reynolds Number [ ]
T	Temperature [C]
th	Thickness [m]
u	Velocity [m/s]
U	Overall Heat transfer coefficient [W/(m^2 K)]
V	Volume flowrate [m^3/s]

Subscripts

a	Air
crit	Critical value
e	Exhausts
EH	Exhausts side

fin	Referred to Fin
g	Gas
HE	Heat Exchanger
i	Referred to i[th] component
in	Inner
L	Laminar
out	Outer
SP	Set Point
std	Standard
U	Overall heat transfer coefficient [W/(m^2 K)]
w	Water
Greeks	
δ	Difference
η	Efficiency
ε	Effectiveness
λ	Height – pitch ratio
σ	Solidity
Acronyms	
HE	Heat Exchanger

1 Introduction

1.1 Waste heat recovery from textile industry

In the last decade, the energy recovery from waste heat flows at low and medium temperature (90-250 ° C) has aroused growing interest, mainly due to the strong push towards energy saving, reducing CO_2 emissions and improving the efficiency of manufacturing processes, industrial and building facilities. The industrial activities, which worldwide account for 38% of primary energy consumption [1], release from 20 to 50% of this energy into waste heat [2]. Cement, glass, metallurgical, food, paper, chemicals and non-metallic minerals are the most intensive sectors. The textile industry, despite being among the least considered, has a relevant overall primary energy consumption (about 87 TWh in USA, [1]) and waste effluent rates levels amongst the highest referred to total input (40%, [1]). In Italy, many industrial sectors reduced their energy intensity since 1995 [3], but food and textiles production had more limited reductions, indicating an interesting potential for relatively unexplored energy recovery in the medium-low temperatures range. Even considering conservative fractions of overall primary national energy input (5-10%), it can be estimated an annual national theoretical availability of waste heat from textiles of the order of 1 – 3 TWh, which rises a significant interest. Fabric finishing represents a relevant share of the primary energy consumption in textile production. In the last years, relevant progresses were done towards waste heat recovery and energy saving in wet processes, whereas much less was done in regards of drying processes involving hot air and/or water flows [4]. Moreover, they are among the most energy – intensive operations in the textile industry and the related waste heat recovery has the potential to significantly reduce the energy consumption of finishing processes [5]. Nevertheless, the issue of waste heat recovery from drying textile machines is not very extensively discussed in literature [4-6], which is preferably oriented towards higher energy-intensive industrial processes.

In textile industrial driers, generally, warm air or combustion gases are impinged on the humid fabric and then vented to the atmosphere: the exhaust stream still has an attractive heat content, which, however, cannot be directly recovered recirculating the exhausts to the process, because they are loaded of humidity and pollutants coming from the fabric (fibres, chemicals and dust). Rather, this heat is recovered through a surface heat exchangers network (recuperators), which exploits the heat content of the exhaust to preheat the fresh dry air to be continuously circulated to the drying process [5, 6].

1.2 Heat exchangers (recuperators)

The current industrial geometry for the exhausts/water heat recuperators is a double concentric pipe, with exhausts in the inner tube and water in the annulus. This is not actually an efficient configuration from the heat transfer point of view, but it is relatively simple, cost effective and easy to periodically clean from the dust and particles carried out from the drying fabric. A finned double pipe configuration would be more effective, especially with a proper design of the fins size and shape. An accurate design is required because the simple geometry of finned tubes can only offer moderate improvements compared to more complicated geometries. On the other hand, the simple solution is appreciated because of the limited cost and easiness of cleaning.

The literature is rich of studies on the performance improvement of double-pipe heat exchangers. In a very recent review [7], the key point appears to be to enhance the overall heat transfer coefficient while minimizing the friction losses; the applied solutions imply surface or geometrical modifications or inserts like turbolators, twisted tapes, extended surfaces etc., which promote the action of secondary flows. When dealing with heat recovery from exhaust gas flows, as for example from Diesel engines, the adoption of gas side finned heat exchangers is convenient because they couple manufacturing simplicity and modest additional costs (compared to simple, less effective bare-pipe configurations) to an appreciable enhancement of the heat transfer effectiveness, at the price of moderate pressure losses

[8]. For this reason, an accurate design of the fins is worth to ensure the highest possible exploitation of the heat exchangers. In this view, Hatami et al. [9] proposed the optimization of an internally finned heat exchanger for the heat recovery from the exhausts of a Diesel engine combining central composite design to CFD. Dealing with CFD techniques as a tool to improve the geometry of finned double pipe heat exchangers, Cavazzuti et al. [10] also remarked that few studies are available on the design and optimization of heat exchangers using the open source code OpenFOAM. They adopted the code to predict the heat transfer rate of finned concentric pipes heat exchangers for industrial recuperative burners. One of few examples is that of Selma et al. [11], who used this code for the optimization of a heat pipe exchanger to improve the energy efficiency of a building ventilation system. However, in a recent review on the use of CFD in heat exchangers design [12] there is no mention on the use of this open source code.

From a survey of the technical literature, it appears that a significant gap exists on the subject of waste heat recovery from commercial fabric drying machines, which are, as above remarked, among the main sources of waste heat in textile industry. On the other hand, the issue of waste heat recovery from exhaust flows is extensively discussed in relation to power plants and boilers for heat generation, but very scarcely for this type of machines, which have specific configurations and technological aspects such as to deserve a detailed analysis in their specific context. It can be thus recommended to investigate the potential savings of the related heat recuperators both from numerical and experimental points of view.

The objective of this study is, therefore, to carry out an accurate analysis of the heat recovery network of a commercial textile dryer by the means of dedicated 0D/3D simulations in the current and redesigned configurations and the subsequent experimental validation of the achieved results.

This objective is pursued by:

1) An accurate design of the heat transfer network and the related heat exchanger modules;
2) The use of the OpenFOAM code to refine the heat exchangers design, which is still at germinal level for industrial cases.
3) The assessed design improvements, which include the overall heat exchanger network as well as the single heat exchangers. They are validated through a test campaign on a dedicated test bench.

2 The heat recovery loop of the industrial fabric drying machine: *Stenter/Rameuse*

2.1 layout of the current commercial configuration

The industrial fabric drying machines (*Stenter/Rameuse*) are long units, typically made of several modules in series (up to 14, generally 7 – 8), each one equipped with a 150 – 200 kWt natural gas burner to warm the air flow by direct mixing with combustion products. Recirculation of the exhaust to the burner is practised, so that the fresh airflow rate is limited to what is needed for combustion, and to the entry of air through the fabric inlet/outlet slots. The machine dries a continuous fabric flow about 2 m wide, which is dragged through a thin slot. The schematic of the texture entrainment and the 3D view of a typical *Stenter/Rameuse* are shown in figure 1.

Often, the dryer also carries out the fabric finishing operations after it has been subjected to previous processes of dyeing and fulling. Direct heat recovery from the exhaust stream to the inlet air (burners and fabric inlet/outlet slots) has proven to be troublesome, due to contamination of the exhaust with dyes, oil and textile fragments; moreover, the air inlet is distributed in several points and this renders, on the whole, this solution unpractical. Thereby, indirect heat recovery systems have been developed, typically recovering heat from the exhaust and transferring it to a water circuit/storage vessel; hot water can then be distributed at heat exchangers for air preheating (typically, located at the inlet/outlet ports; air preheating to the burners is currently not practiced because of the need to use commercial recirculating burners which cannot accept extensive air preheating). Water within the circuit is pressurized (typically to 2-2.5 bar gauge) in order to maintain liquid conditions at temperatures slightly exceeding 100°C. On the upper side of the drying machine (3D view of figure 1b), the heat exchangers/piping network to recover part of the hot exhausts downstream the drying process is shown. The detailed schematic of this part is reported in figure 2 (schematic and pictorial views on left and right respectively).

The heat recuperation from the exhaust stream is done through flow of water across the external annulus of the exhaust pipes; heat is transferred to the air heater at inlet (and possibly outlet, depending on the number of modules of the machine) of the fabric drying process. The basic module for the heat transfer from the exhausts to the drying air is made of 3 counter-current gas/water tube-in-tube heat exchangers. With reference to the cold – water flow, these heat exchangers are currently arranged in series. An air/water heat exchanger (finned type, D in figure 1b, HE_4 in figure 2) preheats the ambient air at the air inlet slots of the machine. The water is circulated by a low-power pump (circulator), which establishes the working flowrate.

Figure 1 – Schematic of the fabric flow and 3D view of the Stenter/Rameuse and of the exhaust heat recovery network

2.2 Data and modelling

The design parameters of the basic configuration module, to which the proposed improved alternatives are referred in the following, start from a few input thermodynamic data available from the manufacturer; all the other thermodynamic parameters of the gas/water/air heat transfer network are calculated as follows by a step-by-step procedure:

1) Definition of the temperatures at suction intakes above the dryer cells (T_9 and T_6), which are input values to the calculation. These are generally measured during operation of the dryer at the design load. Specifically, for the two hot gas flows, different temperatures are registered: the temperature of the first heating section (HE_3 in figure 2) is lower, thus one heat exchanger only (HE_3) is served by this flow.
2) Definition of the volume flow rate at the exhauster output, that is in close relationship to the parameters of the air – water heat exchanger provided by the manufacturer: The flow rate is selected within the working range of the suction fans (variable-speed inverter drive) at a value allowing to match the thermal power and the air flowrate available from the manufacturer's design datasheet of the fresh air/water heat exchanger (HE_4).
3) Input of the water flowrate and output temperature from HE_4 heat exchanger, known from the equipment manufacturer's design datasheet. The flowrate is pre-set at 1.36 kg/s, which determines a laminar regime in the exhausts/water heat exchangers: the water flow is almost steady, with velocity of about 0.04 m/s.
4) Calculation of the exhausts heat exchangers efficiencies (HE_1, HE_2, HE_3) with the NTU-ε method, based on the known surface areas, geometry, inlet temperatures and flow rates, starting from HE_1 where T_2 and T_6 are known. The procedure allows the calculation of the output temperatures (T_7 and T_3 in case of HE_1), which are inputs to the following heat exchanger HE_2. In the same way, applying the NTU-ε method to HE_2, T_8 and T_4 are calculated. The overall heat transfer coefficients U_1, U_2, U_3 are determined based on the flow conditions at both sides of the heat exchangers.
5) Finally, the NTU-ε method applied to HE_3 allows the calculation of the water temperature T_5, which is also known from the HE_4 datasheet: an iterative process was set on the related overall heat transfer coefficient U_4, in order to match the known air/water sides temperatures and flowrates and the overall heat transfer surface area of HE_4.

The complete 0-D procedure allows to determine all parameters of the heat exchangers network and the thermodynamic data at the various points of the circuits under typical design working conditions of the dryer. The input data and results of calculation are summarized in tables 1and 2.

The 0-D calculations are performed with an in house developed EES model [13], a calculation environment specifically suitable for this kind of applications, because of its numerous built-in procedures dedicated to heat transfer problems, also involving heat exchangers with complex geometry. With indexes referred to the scheme and subscripts w, e and a for the water, exhausts and air respectively, the main governing equations are resumed in the following.

Mass balance on the lines of water, exhausts and air:

$$m_1=m_2=m_3=m_4= m_w \quad (1)$$

$$m_6= m_7= m_8=m_{e1} \quad (2)$$

$m_{10}=m_9=m_{e2}$ (3)

$m_{13}=m_{12}=m_a$ (4)

The calculations apply the *NTU-ε method* [14] to determine the unknown parameters, starting from those known for the different heat exchangers according to the manufacturer's data:

$C_{e,i}= m_{e,i}\cdot cp_{e,i}$ exhaust side heat capacity; (5)

$C_{w,i} = m_{w,i}\cdot cp_{w,i}$ water side heat capacity; (6)

$C_{min,i} = \min(C_{e,i}; C_{w,i})$ minimum heat capacity; (7)

$Q_{max,i} = C_{min,i}\,(T_{e,i} - T_{w,i})$ minimum heat capacity; (8)

$NTU_i = U_iA_i/C_{min,i}$ number of thermal units; (9)

The efficiency ε is calculated with the internal EES heat transfer library functions, which make use of the well-known NTU-ε relationships as function of heat capacitance rate $C_{min,i}/ C_{max,i}$ [14]. The overall heat transfer coefficient U_i is also calculated with the EES internal functions, considering external flow on the water side (annulus between the two concentric pipes) and the internal pipe flow on the exhausts side. For the calculation of friction losses, correlations for laminar, transitional and turbulent flow were used. For turbulent pipe flow, the friction factor f_i, in case of relative roughness between 0 and 10^{-5} (*smooth tubes*) is calculated with the Seem and Li correlation [15]; in case of relative roughness higher than 10^{-5} (*rough tubes*) f_i is calculated with the Zigrang and Sylvester correlation [16]. The Nusselt number Nu_i is calculated with the Gnielinski correlation [17].

In case of laminar flow, correlations for the Darcy friction factor on developing and fully developed flow regions, available on Shah and London [18], are adopted.

Figure 2 – Schematic of the current heat exchanger network of the Stenter/Rameuse

Table 1 shows the known input data from the manufacturer's datasheet for typical operation of the *Stenter/Rameuse*; the assumed unknown values and calculation model's output are checked in feedback to tune the model's parameters. Table 2 shows the main heat exchangers parameters. The numerical indexes are referred to the top left scheme of figure 2.

Table 1 – Main data of the current heat recovery network and heat exchangers parameters

Table 2 – Main current heat exchangers parameters

3 New layout of the heat recovery network

The new proposed layout of the heat recovery network, as well as the enhanced data, are shown in figure 3 and tables 3 and 4 (system components and heat exchangers respectively). The main difference is the parallel arrangement for the water circuit, realized using two manifolds (delivery 3 and return 4); each exhaust heat exchanger is fed in parallel connecting to these manifolds. Moreover, the heat transfer on the exhausts side is improved by splitting the original single can into two twin-can exhaust channels with reduced diameters carrying equal mass flowrates. In this way, with the same fixed cross flow section area, the heat transfer surface is significantly increased. This plays a fundamental role in augmenting the gas side heat transfer, which is strongly limited by the low heat transfer coefficient.

In order to allow an efficient access for cleaning of the internal exhausts ducts, the pipe size can be only moderately reduced: the investigated diameters of the twin cans were 0.2, 0.22 and 0.25 m (labelled as C.200, C.220 and C.250 respectively) as an alternative to the 0.35 m of the current single-pipe configuration (A.350).

Further improvement of heat transfer is achieved by adding fins on the internal surface of the twin ducts (gas side). As the internal fins are manufactured and assembled (as described in the following), it was decided to adopt a shorter length of each module, realizing each barrel of the two cans with two modules in series (2x0.986 m). The resulting overall length is slightly lower compared to the original one (2.283 m), in order to leave space for the connecting flanges, see figures 2 and 3. The pipe is realized by calendering of a metal sheet manufactured by laser cutting. The fins are longitudinal, positioned with studs on the pre-perforated plate. The size and the maximum number of fins in the channel are defined by the solidity $\sigma_{fin}=N_{fin}\cdot th_{fin}/(\pi\cdot D_{in})$ and the height to pitch fin ratio $\lambda_{fin}=H_{fin}/(Ptc_{fin}-th_{fin})$ inside the channel. In order to improve the overall heat transfer, the current stainless steel solution was replaced with carbon steel. After placing the fins, a galvanizing process eliminates the fin/pipe contact resistance and ensures corrosion protection. At the same time, the zinc coating significantly increases the surface roughness compared to that of stainless steel (from 0.01 to about 0.046 mm), thus increasing the overall heat transfer coefficient between 4.5 and 6%.

The 0D calculation model adopted for the annular water/gas heat exchangers of each single can is similar as discussed in section 2 for the current commercial configuration with bare tubes. The main difference is the introduction of N_{fin}

longitudinal fins, whose efficiency η_{fin} is calculated by an internal procedure referred to rectangular shaped fins as a function of its dimensions (H_{fin}, L_{fin}), material conductivity k_{fin} and heat transfer coefficient h_{fin} between the flow and the fin surface [13]. The latter is calculated with the following correlation between the Nusselt number (Nu_{fin}), Reynolds (Re_{fin}) and Prandtl (Pr_{fin}) numbers:

$$Nu_{fin} \frac{0.6774\, Pr^{1/3} {Re_{crit}}^{1/2}}{\left[1+\left(\frac{0.0468}{Pr}\right)^{2/3}\right]^{1/4}} + 0.037\, Pr^{\frac{1}{3}} (Re_L^{0.8} - Re_{crit}^{0.8}) \quad [14] \qquad (10)$$

$$h_{fin} = k_{fin} Nu_{fin} / L_{fin} \qquad (11)$$

Thus, the additional heat recovered using fins on the exhausts side is given by:

$$Q_{fin} = \eta_{fin} h_{fin} H_{fin} L_{fin} (T_{e,i} - T_{w,i}) \qquad (12)$$

Figure 3 – Layout of the improved heat recovery loop

Table 3 – Main circuit data of the improved heat recovery network

Table 4 – Main heat exchangers data of the improved heat recovery network

4. Comparison of the proposed solutions

The comparison of the proposed solutions and the selection of the best one is done referring to the current basic commercial case with one single duct. The identifier codes, features and relevant dimensions of the different solutions are summarized in table 5. The analysis is done for three different values of the water mass flowrate: 4, 8 and 16 l/s, in order to assess the influence of the corresponding flow velocity in the annulus, whose increase gives a further contribution to the heat transfer from hot gas to cold water.

The adoption of twin-can heat exchangers leads to an increase of gas and water velocity, as shown in figure 4.

The comparison of the twin-can configurations C.250, C.220, C.200 at variable flowrate in the water loop and for different number of fins is shown in figure 5 a) and b), in terms of heat transferred and temperature of the water and exhausts at points 5 and 11 (referred to figure 3). It can be noticed that generally - as expected - the increase in number of fins leads to a higher heat recovery (figure 5 a), which is also confirmed by the corresponding increase of water temperature and decrease of exhaust temperature (figure 5 b). This is also in agreement with the general trend found in [9] for a geometrically similar case.

The modifications introduced determine a remarkable increase of the heat transferred compared to the current commercial bare pipe single can configurations. In particular, there is a considerable improvement in the C.220 and C.200 configurations.

Table 5– Main parameters of the original and improved water/gas heat exchangers

Figure 4 – Gas and water velocities in the different analysed cases

The twin cans give a better reconfiguration to the heat recovery network, while the fins increase the heat transfer potential of each single pipe. The cumulative contributions of the modifications on the overall power output of the heat recovery network, compared to the base case A.350, are shown on figure 6. The adoption of the twin can arrangement has a prevailing effect at low diameters (C.200/F series) and higher water mass flowrates, due to the reduced available space, which limits the maximum applicable number of fins on the inner surface of the pipes. As shown on figure 5a, the heat recovery increases from C.250/F through C.220/F to C.200/F: the explanation is that the gas velocity is larger and thus the gas side heat transfer coefficient. However, 220 mm was considered as the lowest acceptable diameter for cleaning issues.

The twin-can configuration with fins increases the friction losses compared to the single bare pipe one of the current commercial version of the heat recovery circuit. They were evaluated, in terms of head loss and required fan power, with the calculation model described in section 2. In the original configuration, about 20 Pa head losses per module due to friction were calculated on the exhausts side, which require about 39 W fan power, for a total of 117 W (see data on Table 2). In the C.220/F with 16 fins, the calculated pressure drop per module is 130 – 143 Pa, requiring a total 596 W fan power (183 to 208 W per each HE, see Table 4). This is relatively a great increment, but, in absolute terms, the additional 479 W of mechanical power produce an increase of about 45 kW in heat recovery.

Figure 5 – Heat rate of HE4 and water/exhausts temperatures(comparison of cases C.xxx/20/2)

Figure 6 – Cumulative effect of the modifications introduced in the heat recovery network (comparison of cases C.xxx/30/3)

5 Detailed CFD design and analysis of the twin-can heat recovery module

After the sizing of the internally finned gas/water heat exchangers, a detailed refined design of the single module of twin-can water/gas heat exchanger was performed. Specifically, the influence of shape, size and thickness of the fins on the performance of the heat exchanger module were analysed with a CFD approach developed in OpenFOAM environment. The computational mesh was created with the *SnappyHexMesh* application (structured grids) with resolution ranging from about 3.7 to 5.1 million points. The numerical simulations were run for stationary flow and the problem was solved by the conjugate heat transfer solver *chtMultiRegionSimpleFoam* with 2nd order schemes for discretization terms and *k-Omega SST* as turbulence model. Table 6 summarizes the resolution, features and thermodynamic parameters of the CFD model.

Table 6 – CFD Model Data

Following are the key issues of the finned heat exchanger module design:

- Increased internal heat transfer (gas side);
- Effective increase of the fin-tube contact surface;
- Improved turbulence conditions;
- Guaranteed easy cleaning of the finned internal exhaust gas side.

In order to meet these objectives, the thermal behaviour of five possible fins configurations, different in size and/or geometry and disposal, are analysed and compared each other. Specifically, the following configurations were examined (see schematics in figure 7):

1) ***Continuous straight fins*** with different thickness and height (C.220/20/2/1F, C.220/25/3/1F, C.220/30/3/1F);
2) ***Interrupted fins*** (C.220/20/2/9F);
3) ***Shifted segmented fins*** (C.220/30/3/3F).

The geometric details, codes and type of analysis of all the configurations are summarised in figure 7. The performance of the heat exchanger was compared to those of the basic bare tube (C.220).

The 2D temperature cross sectional distribution around the different investigated fins are summarised in figure 8: the growth of thermal boundary layer in the flow direction is evident in the three representative cross sections along the z axis. It is only moderately influenced by the fin height, passing from 20 to 30 mm. By the way, the influence of fin thickness is marginal.

The effect of straight fin segmentation (case C.220/20/2/9F) is shown in figure 9, reporting the behaviour of the temperature fields on the longitudinal axial section (z) in the two cases of continuous and interrupted fins. The advantages related to the adoption of interrupted fins are marginal. The reason is the not efficiently renovated build-up of the thermal boundary layer around the fin, even with frequent interruptions. This effect is remarked in the close-up of temperature distribution in two different axial positions of figure 9): close to the inlet (1) and to the outlet (2). This effect is also confirmed by the behaviour of heat flux decay for the two cases in the xz midspan section, which is practically the same in the first 30% of the axial path. The values in the marked sections are reported and compared in table 7.

The most significant improvement of performance in heat transfer is achieved with the adoption of three radially shifted segmented fins (C.220/30/3/3F). In fact, radial shifting of the fins (7.5°) guarantees an effective renovation of the thermal boundary layer. The length of the fin is adequate to prevent the development of a thermally exhausted film over the fin.

The satisfactory results can be quantitatively evaluated in terms of temperature profiles (figure 10) and heat flux (figure 11) on the midspan section. In the latter, the effect of heat flux recovery on the leading edge of each fin is well noticeable.

Figure 7 – schematic of geometry, size, and cross sectional mesh of the different investigated fin

Figure 8 – Cross sectional flow of the heat exchanger module with the different investigated fins

Table 7– Comparison of heat fluxes along the xz midspan section between continuous and interrupted fins

Figure 9 – Temperature field and heat flux distributions in the axial xz midspan section for interrupted and continuous fins

Figure 10– Temperature profile on the midspan section in the case of 3 shifted segmented fins (C.220/30/3/3F)

Figure 11– Heat flux profile on midspan section in the case of 3 shifted segmented fins (C.220/30/3/3F)compared to the case with single continuous fin

Figure 12 shows the temperature profile in the axial direction of the different fins at two different heights Y (referred to the axis of the duct, thus increasing from the tip to the hub of the fin). The effective renovation of the thermal boundary layer with shifted fins is evident: with the continuous fins, the temperature gradient is high at the leading edge and for the first 10% of axial distance. Successively, the thermal boundary layer "relaxes" and the temperature gradient is strongly reduced. The behaviour is similar for fins of different height and thickness. The influence of fin height on the values of temperature profile is appreciable, whereas that of fin thickness is marginal. The effect of thermal boundary layer renovation is also evident in the case of interrupted fins (C.002/02/9F), but it is relatively modest and allows only a moderate improvement over the continuous fins, as discussed (figure 9 and table 7).

Figure 12– Axial temperature profile of the different fins at two fin height (tip and hub)

The results achieved with 3D CFD analysis applied to the bare and finned pipes were also compared to those of the 0D models discussed on section 3, which adopts correlations to calculate the overall heat transfer parameters. With reference to the bare pipe, figure 13 shows, for example, the comparison of the heat flux profiles of the hot exhaust streamside along the axis of the single heat exchanger module calculated with the OpenFOAM CFD (averaged) and the EES model.

Figure 13- Heat flux profile of the hot exhausts flow at the HE module

Finally, the overall heat recovered per module of the twin-can heat exchanger with the different types of fins is reported on table 8, as well as the comparison with the results achieved with the 0D model in the cases where it is applicable (i.e. not in the case of shifted fins). Compared to the heat recovered with the bare pipe, the improvement due to fins is well evident, ranging from a minimum of 53% with the interrupted fins (C.220/20/2/9F) to the 97% of the three shifted segmented fins (C.220/30/3/3F).

The agreement between the results achieved with CFD and 0D correlation models is satisfactory, with relative errors between 1.5 and 2.7%.

Table 8– Heat recovered with the different kinds of fins and comparison between 3D CFD and 0D results

6 Experimental setup and tests

A dedicated experimental setup (figure 14), consisting in one fully instrumented module of the drying machine, was realized to check the correctness, operability, reliability and effectiveness of the proposed redesign solutions to improve the heat recovery section.

A test campaign was organized on the heat exchangers modules with shifted fins (*C.220/30/3/3F*), mounted on the twin can HE arrangement (figures 14 and 15). The purpose of the tests was:

a) To validate the predicted performance of the single heat recovery module (0D and 3D models).

b) To verify that the twin-can water manifold arrangement was working correctly, with even flow distributions between parallel branches for all operating conditions.

c) To verify the optimizing conditions of the whole machine (burner, exhaust and heat recovery network setup) with variable control settings.

The test conditions should reflect the real operation of the machine. Therefore, several values of set point temperature T_{SP} were considered. T_{SP} is the temperature at the entrance of the *Stenter/Rameuse* section, which is the main parameter that a textile producer can adjust depending on the fabric processing parameters.

Figure 14– view of the experimental setup of the rameouse cell equipped with twin-can recuperator module

For each value of T_{SP}, the test bench allowed some degrees of freedom, which are reflected in the control strategy and can be implemented on the real machine. In detail, three inverters are available: A) on the exhaust fan, regulating the air passing through the textile drier; B) on the circulation pumps of the water circuit; C) on the water-air heat exchanger fan. When operating the machine, increasing the exhaust gas flow rate (A) improves the heat transfer (which depends on the exhaust gas velocity); however, more air is entrained through the fabric entrance slots, and this determines a higher consumption of natural gas for the burner in order to maintain the value of T_{SP}. Moreover, the exhaust fan has a power rating of 6 kW, considerably larger than power absorbed by the circulation pumps (B) or by the air preheat fan (C). Consequently, the operator tries to maintain a value of exhaust flow rate as low as possible compatibly with the stability of operation (2930 Sm^3/h in the reference test conditions). Heat recovery performance optimization is rather sought adjusting the speeds of the pumps (B) or of the air fan (C).

The test bench was designed to confirm uniformity of performance for the two branches in parallel; consequently, both branches were completely instrumented. In order to estimate the heat recovered by the heat exchangers, 8 Platinum thermo-resistance probes (PT100) with 1/10 DIN accuracy (0.1 °C) were placed on the water circuit, as displayed in figure 15(T_{11} to T_{31} on the lower branch; T_{12} to T_{32} on the higher branch; T_{13} and T_{23} at the entrance and exit of the water-air heat exchanger). 3 PT100 were set on the exhaust gas circuit (T_{g1}; T_{g2}; T_{g3}). T_{g2} was a special shielded total temperature probe, designed to provide reliable measurements within the inner exhaust pipe (the probe design includes velocity control minimizing recovery error, and radiation shielding); on the other hand, due to layout problems, probes T_{g1} and T_{g3} were simple bare sensor probes inserted in branching connections, installed mainly for a qualitative check than for accurate measurements. An electromagnetic flow meter with 0.5% actual value accuracy was placed at the inlet of the two heat exchanger branches to measure the water mass flow rate (m_1, m_2) and a calibrated orifice with differential pressure transducer and temperature measurement measured the exhaust outlet gas flow rate.

Figure 15– cross section of the realized pipe module, rendering view of the heat exchangers assembly and schematic of the experimental setup

The results confirmed that the exhaust flow was evenly distributed in the two branches at all operating conditions; consequently, the evaluation of the performance is reported for one single module (namely, HE_1), and for the complete unit (4 heat recovery modules, piping and water/air heat exchanger). Table 9 and figure 16 display the experimental results obtained against the simulation results. In particular, the heat rate and the temperature at the exit of heat exchanger 1 (HE_1; operating with lower average exhaust gas temperature) are shown. The accuracy of prediction of water temperature is very good (globally less than 0.5°C difference between simulation and measurements). On the other hand, the simulated and measured heat rates present some deviations, which are due mostly to the fluctuation of the exhaust gases temperature and especially by its flow rate. The tests confirmed that – depending on the system operating conditions – the low-temperature gas exhaust recovery heat exchanger module is typically capable of recovering from 3.5 to 5.5 kW, which is in line with the model predictions (Table 8).
During the tests, it was clear that the air circulation fan (C) should be operated at the highest speed in order to improve the heat transfer in the air/water heat exchanger. However, optimizing conditions did exist for the water flow rate. Figure 17 displays how the whole heat exchanger network operates varying both water mass flow rate and set point temperature. The heat recovered presents a maximum for values of the total water mass flow rate around 15 l/min. This is because at lower values of water flow rate the liquid-side convection transfer coefficient becomes very low. On the other hand, at higher values of water flow rate, the temperature difference between inlet and outlet of the heat exchanger becomes smaller, as the water returning to the gas/water heat exchanger has a higher temperature, thereby hindering the heat transfer. This is a whole system effect, determined by combined operation of the heat recovery network (gas/water and air/water heat exchangers) and the constraints imposed by the set point conditions. The performance of the isolated

heat exchanger module, as predicted with the calculation models, would continue to increase with increasing velocity/flow rate of water.

Table 9– Heat Recovery of HE_1 comparison between experiments and simulation

Figure 16– Water Temperature at outlet of HE_1 comparison between experiments and simulation

Figure 17– Heat Exhanger network operation map

7 Conclusions

The heat recovery system of an industrial textile dryer (*Stenter/Rameuse*) was redesigned looking after general performance improvement. The redesign procedure followed three main steps:

1) Thermodynamic analysis of the current heat recovery section, with rearranged manifold layout of the heat exchangers network making use of heat transfer correlations;
2) Detailed CFD analysis of the proposed heat exchangers modules and design/manufacturing of the final prototypes;
3) Experimental campaign on one stenter module, in order to verify the correctness and reliability of the predicted results from the 0D and CFD calculations.

The key results of the study may be summarized as follows:

- The 0D (heat transfer correlation) model proved to be effective to examine the fundamental design alternatives, allowing to predict the possibility of extensive heat recovery from the low-temperature exhaust gases.
- The improved layout of the water/exhausts heat recovery circuit proposes a parallel manifold arrangement of the water circuit; in order to increase the heat transfer surface area and the exhausts velocity, an internally longitudinally finned twin-can configuration of the heat exchangers was proposed.
- The adoption of a twin-can geometry with 16 fins leads to a heat recovery potential almost doubled with reference to the current basic configuration: the contribution of twin cans ranges from 25 to 35%, whereas that of fins ranges from 40 to 50%, the latter increasing when the diameter of the pipes is reduced. On the whole, the heat recovery potential was estimated to increase of about 180 % over the original configuration with

single bare pipes in series (45 kW more), at the moderate price of 480W additional mechanical power of fans due to increased friction.

- The detailed design of the new twin can heat exchangers with 16 fins was performed applying CFD in OpenFoam environment: this allowed the evaluation of the influence of shape, size and fins thickness on the heat exchanger performance:
  - The highest performance improvement of the heat exchanger module was achieved in the configuration with three shifted segmented fins, due to the effective renovation of the thermal boundary layer, which leads to a remarkable recovery of heat flux on the leading edge of each fin and then “relaxes” in the following. The influence of fin height on heat flux recovery is moderate, while that of fin thickness is marginal.
  - The overall heat recovered with the 5 different analysed fin configurations range from 53 to 97%, in agreement with the levels predicted by the zero dimensional EES calculation models.
- The results of the models were operationally validated on a test bench, reproducing one full-scale section of the Stenter; the purpose of the tests was not only to validate the model predictions (accuracy of prediction of water temperature within 0.5°C between simulations and measurements), but also to verify the correct operation of the dual-can water manifold arrangement, and to identify control strategies for the burner/ air/gas/water flow rate control settings, depending on the nominal temperature set point of the machine. The tests gave positive issues, validating the model predictions, confirming correct operability of the unit and identifying the correct control strategy.

Acknowledgements

Help and workshop/test bench supervision by Ing. Guido Giorgetti of Unitech Textile Machinery is gratefully acknowledged for providing drawings, data and measured working conditions of the reference case study.

The experimental setup and analysis has been funded by Regione Toscana, project ***MPENMAT***, funds PRSE 2012-2015 -line 1.1b - POR CREO FESR 2007-2013 line 1.3b - POR CREO FESR 2014-2020 Action 1.1.2 A – Support to theSMEsfor innovation services.

References

[1] U.S. Energy Information Administration, 2013. International energy outlook 2013. Available at: http://www.eia.gov/outlooks/ieo/pdf/0484(2013).pdf(accessed 06.01.17).

[2] Tello, P. and Weerdmeester R., 2013. Spire Roadmap. Available at: https://www.spire2030.eu/sites/default/files/pressoffice/spire-roadmap.pdf(accessed 06.01.17).

[3] ENEA, 2015, RAEE -RapportoAnnualesull'EfficienzaEnergetica. Available at:http://www.enea.it/it/pubblicazioni/pdf-volumi/raee-2015.pdf(accessed 06.01.17).(in Italian)

[4] Pulat, E.,Etemoglu, A.B., Can, M.,2009. Waste-heat recovery potential in Turkish textile industry: Case study for city of Bursa. In: Renewable and Sustainable Energy Reviews, 13 (3),663-672.

[5] TuğrulOğulata, R., 2014. Utilization of waste-heat recovery in textile drying. In: Applied Energy, 79 (1), 41-49.

[6] Rakib, M.I.,Saidur,R.,Mohamad, E.N.,Afifi, A.M.,2017. Waste-heat utilization – The sustainable technologies to minimize energy consumption in Bangladesh textile sector. In: Journal of Cleaner Production, 142 (4), 1867-1876.

[7] Omidi, M.,Farhadi, M.,Jafari, M.,2017. A comprehensive review on double pipe heat exchangers. In: Applied Thermal Engineering, 110, 1075-1090.

[8] Hatami, M.,Ganji, D.D.,Gorji-Bandpy, M., 2014. A review of different heat exchangers designs for increasing the diesel exhaust waste heat recovery. In: Renewable and Sustainable Energy Reviews, 37, 168-181.

[9] Hatami, M., Jafaryar, M.,Ganji, D.D.,Gorji-Bandpy, M., 2014. Optimization of finned-tube heat exchangers for diesel exhaust waste heat recovery using CFD and CCD techniques. In: International Communications in Heat and Mass Transfer, 57, 254-263.

[10] Cavazzuti, M.,Agnani, E., Corticelli, M.A.,2015. Optimization of a finned concentric pipes heat exchanger for industrial recuperative burners. In: Applied Thermal Engineering, 84, 110-117.

[11] Selma, B.,Désilets, M., Proulx, P., 2014. Optimization of an industrial heat exchanger using an open-source CFD code. In: Applied Thermal Engineering, 69 (1–2), 241-250.

[12] Bhutta, M.M.A., Hayat, N., Bashir, M.H., Khan, A.R., Ahmad, K.N., Khan, S., 2012. CFD applications in various heat exchangers design: A review. In: Applied Thermal Engineering, 32, 1-12.

[13] Klein, S.A., 2016. Engineering Equation Solver (EES), Academic Professional V10-095-3D (7/11/16), © 1992-2016.

[14] Nellis, G., and Klein, S.A., 2009. Heat Transfer. Cambridge University Press, New York, NY.

[15] Li, P., Seem, J.E., Li, Y., 2011.A new explicit equation for accurate friction factor calculation of smooth pipes. In: International Journal of Refrigeration, 34 (6) 1535-1541.

[16] Zigrang, D.J. and Sylvester, N.D., 1982. Explicit approximations to the solution of Colebrook's friction factor equation. In:AIChE Journal, 28, 514-515.

[17] Gnielinski, V., 1976. New Equation for Heat and Mass Transfer in Turbulent Pipe and Channel Flow. In: International Chemical Engineering, 16, 359-368.

[18] Shah, R.K. and London, A.L., 1978. Laminar Flow Forced Convection in Ducts, Academic Press.

Figures captions

Figure 1 – Schematic of the fabric flow and 3D view of the *Stenter/*Rameuse and of the exhaust heat recovery network

a) Schematic of the drying texture flow

b) 3D view of the *Stenter/*Rameuse and exhausts heat recuperation loop

Figure 2 – Schematic of the current heat exchanger network of the *Stenter/*Rameuse

Figure 3 – Layout of the improved heat recovery loop

Figure 4 – Gas and water velocities in the different analysed cases

Figure 5 – Heat rate of HE4 and water/exhausts temperatures(comparison of cases C.xxx/20/2)

a) Absolute Heat power of HE_4 and comparison with the current base case

b) Water and exhausts temperature at points 5 and 11

Figure 6 – Cumulative effect of the modifications introduced in the heat recovery network (comparison of cases C.xxx/30/3)

Figure 7 – schematic of geometry, size, and cross sectional mesh of the different investigated fins

Figure 8 – Cross sectional flow of the heat exchanger module with the different investigated fins

Figure 9 – Temperature field and heat flux distributions in the axial xz midspan section for interrupted and continuous fins

Figure 10 – Temperature profile on the midspan section in the case of 3 shifted segmented fins (C.220/30/3/3F)

Figure 11 – Heat flux profile on midspan section in the case of 3 shifted segmented fins (C.220/30/3/3F)compared to the case with single continuous fin

Figure 12 – Axial temperature profile of the different fins at two fin height (tip and hub)

Figure 13 - Heat flux profile of the hot exhausts flow at the HE module

Figure 14 – View of the experimental setup of the rameouse cell equipped with twin-can recuperator module

a) Front view

b) Back view

Figure 15 – Cross section of the realized pipe module, rendering view of the heat exchangers assembly and schematic of the experimental setup

a) Cross section of the realized pipe module of the twin-can HE with internal shifted fins (C.220/30/3/3F)

b) New heat exchangers assembly with twin-can HE modules

c) Schematic of the experimental setup of the twin-can HE

Figure 16 – Water Temperature at outlet of HE_1 comparison between experiments and simulation

Figure 17 – Heat Exhanger network operation map

Tables captions

Table 1 – Main data of the current heat recovery network and heat exchangers parameters

Table 2 – Main current heat exchangers parameters

Table 3 – Main circuit data of the improved heat recovery network

Table 4 – Main heat exchangers data of the improved heat recovery network

Table 5 – Main parameters of the original and improved water/gas heat exchangers

Table 6 – CFD Model Data

Table 7 – Comparison of heat fluxes along the xz midspan section between continuous and interrupted fins

Table 8 – Heat recovered with the different kinds of fins and comparison between 3D CFD and 0D results

Table 9– Heat Recovery of HE_1 comparison between experiments and simulation

Figures

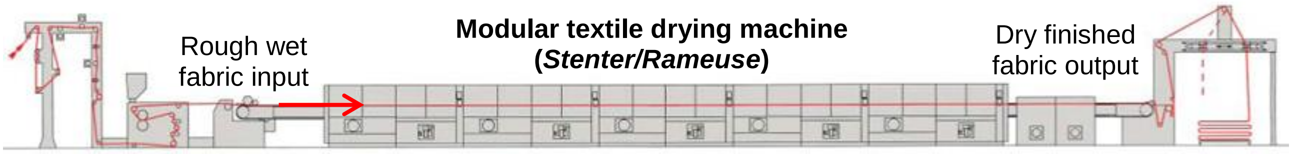

a)

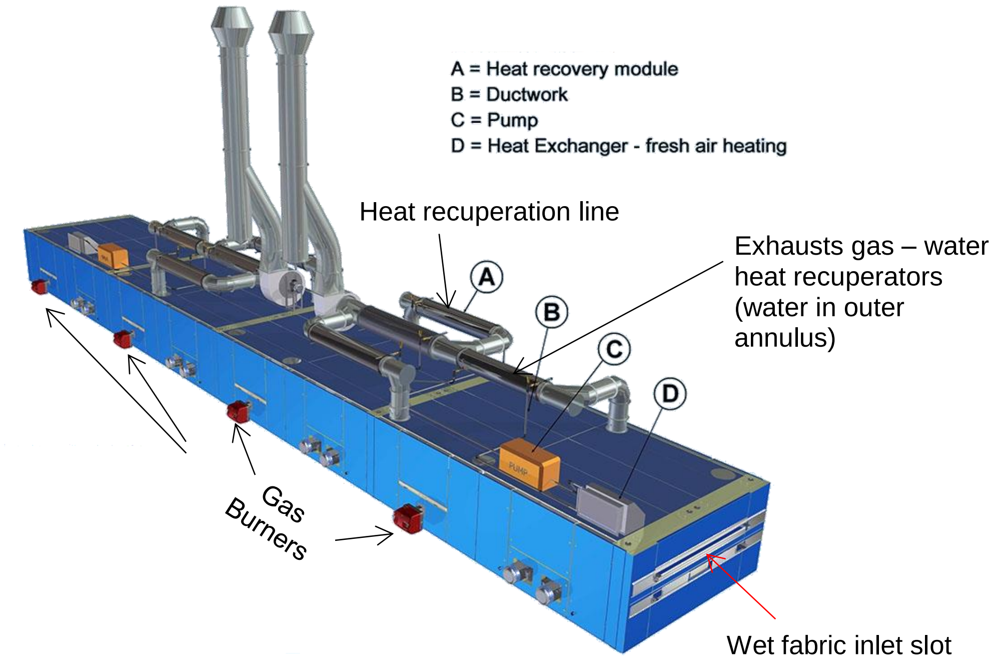

b)

Figure 1

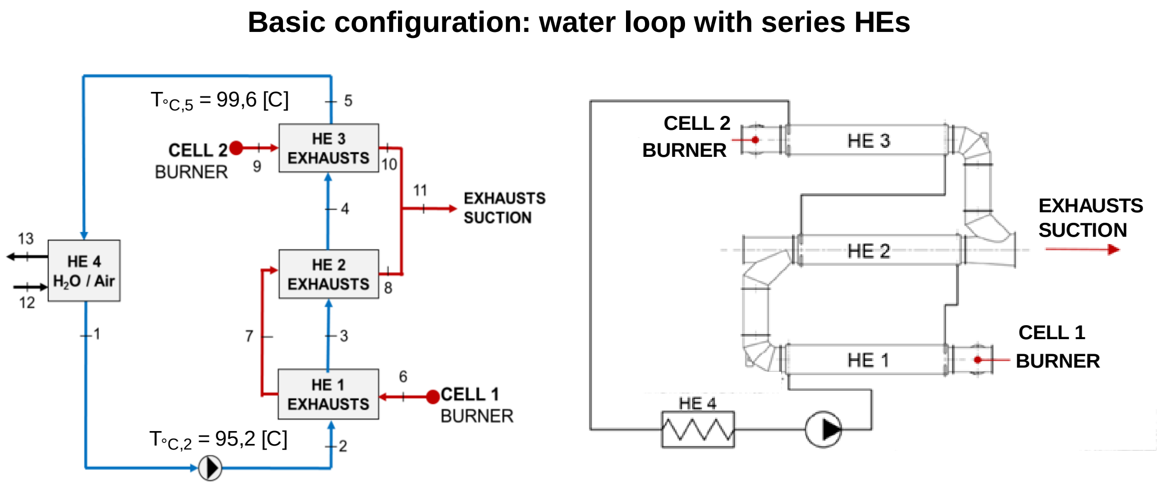
Basic configuration: water loop with series HEs
T°C,5 = 99,6 [C]
5
HE 3
EXHAUSTS
CELL 2
BURNER
9
10
11
EXHAUSTS
SUCTION
4
13
HE 4
H2O / Air
12
HE 2
EXHAUSTS
8
1
7
3
HE 1
EXHAUSTS
6
CELL 1
BURNER
T°C,2 = 95,2 [C]
2
CELL 2
BURNER
HE 3
HE 2
EXHAUSTS
SUCTION
HE 1
CELL 1
BURNER
HE 4

Figure 2

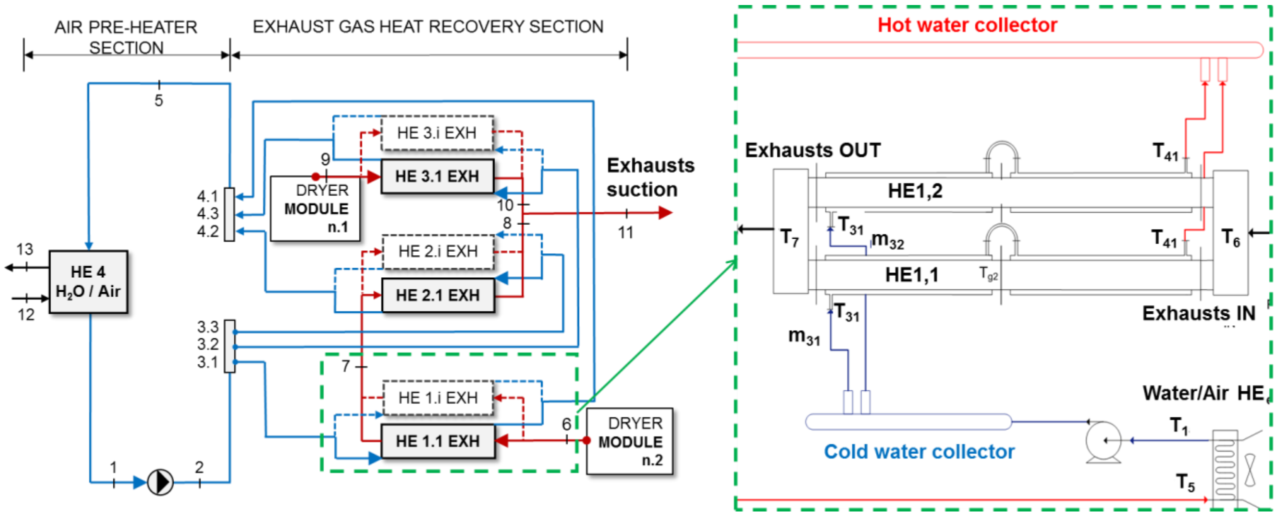
AIR PRE-HEATER SECTION
EXHAUST GAS HEAT RECOVERY SECTION
HE 4 H_2O / Air
HE 3.i EXH
HE 3.1 EXH
HE 2.i EXH
HE 2.1 EXH
HE 1.i EXH
HE 1.1 EXH
DRYER MODULE n.1
DRYER MODULE n.2
Exhausts suction
Hot water collector
Exhausts OUT
HE1,2
HE1,1
Exhausts IN
Water/Air HE
Cold water collector
T_{41}
T_7
T_{31}
m_{32}
T_6
m_{31}
T_1
T_5

Figure 3

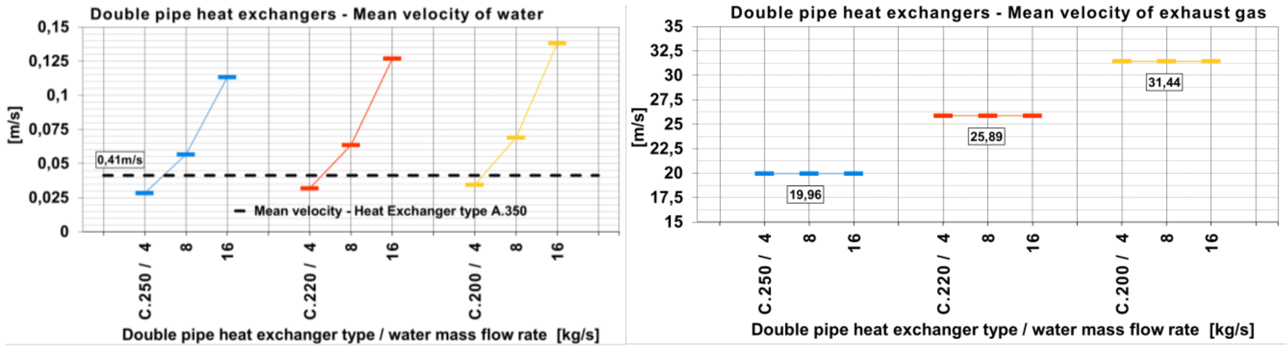

Double pipe heat exchangers - Mean velocity of water
[m/s]
0,15
0,125
0,1
0,075
0,05
0,025
0
0,41m/s
Mean velocity - Heat Exchanger type A.350
C.250 / 4
8
16
C.220 / 4
8
16
C.200 / 4
8
16
Double pipe heat exchanger type / water mass flow rate [kg/s]
Double pipe heat exchangers - Mean velocity of exhaust gas
[m/s]
35
32,5
30
27,5
25
22,5
20
17,5
15
19,96
25,89
31,44
C.250 / 4
8
16
C.220 / 4
8
16
C.200 / 4
8
16
Double pipe heat exchanger type / water mass flow rate [kg/s]

Figure 4

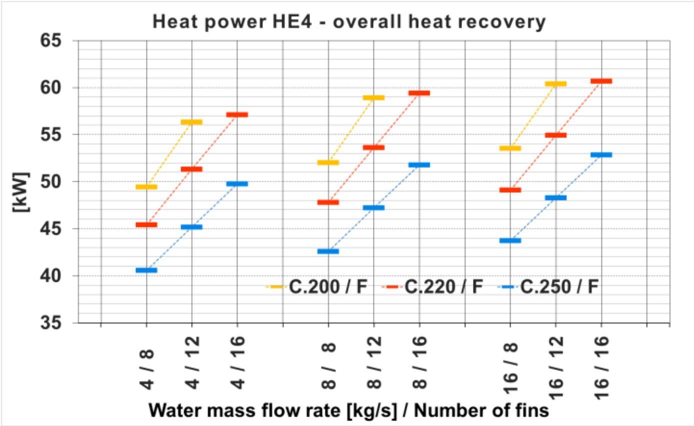
Heat power HE4 - overall heat recovery
[kW]
65
60
55
50
45
40
35
C.200 / F
C.220 / F
C.250 / F
4 / 8
4 / 12
4 / 16
8 / 8
8 / 12
8 / 16
16 / 8
16 / 12
16 / 16
Water mass flow rate [kg/s] / Number of fins

a)

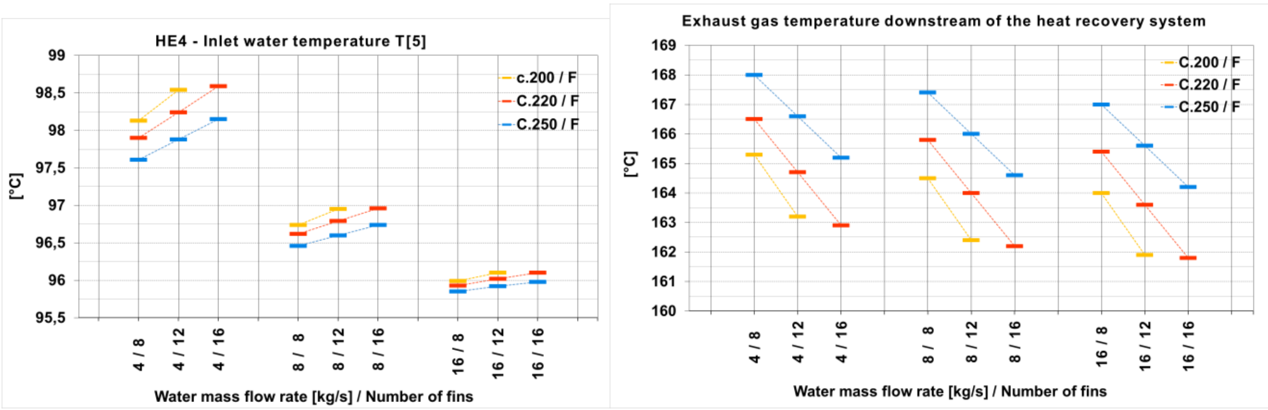
HE4 - Inlet water temperature T[5]
[°C]
99
98,5
98
97,5
97
96,5
96
95,5
c.200 / F
C.220 / F
C.250 / F
4 / 8
4 / 12
4 / 16
8 / 8
8 / 12
8 / 16
16 / 8
16 / 12
16 / 16
Water mass flow rate [kg/s] / Number of fins
Exhaust gas temperature downstream of the heat recovery system
[°C]
169
168
167
166
165
164
163
162
161
160
C.200 / F
C.220 / F
C.250 / F
4 / 8
4 / 12
4 / 16
8 / 8
8 / 12
8 / 16
16 / 8
16 / 12
16 / 16
Water mass flow rate [kg/s] / Number of fins

b)

Figure 5

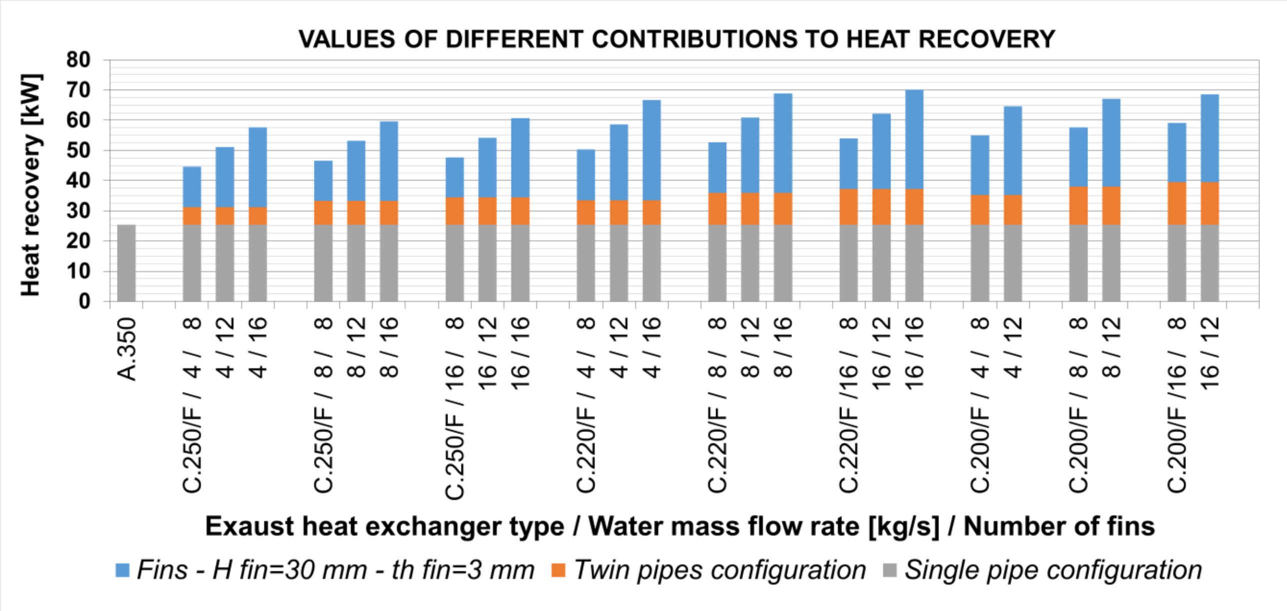
VALUES OF DIFFERENT CONTRIBUTIONS TO HEAT RECOVERY
Heat recovery [kW]
Exaust heat exchanger type / Water mass flow rate [kg/s] / Number of fins
A.350
C.250/F / 4 / 8
4 / 12
4 / 16
C.250/F / 8 / 8
8 / 12
8 / 16
C.250/F / 16 / 8
16 / 12
16 / 16
C.220/F / 4 / 8
4 / 12
4 / 16
C.220/F / 8 / 8
8 / 12
8 / 16
C.220/F /16 / 8
16 / 12
16 / 16
C.200/F / 4 / 8
4 / 12
C.200/F / 8 / 8
8 / 12
C.200/F /16 / 8
16 / 12
Fins - H fin=30 mm - th fin=3 mm
Twin pipes configuration
Single pipe configuration

Figure 6

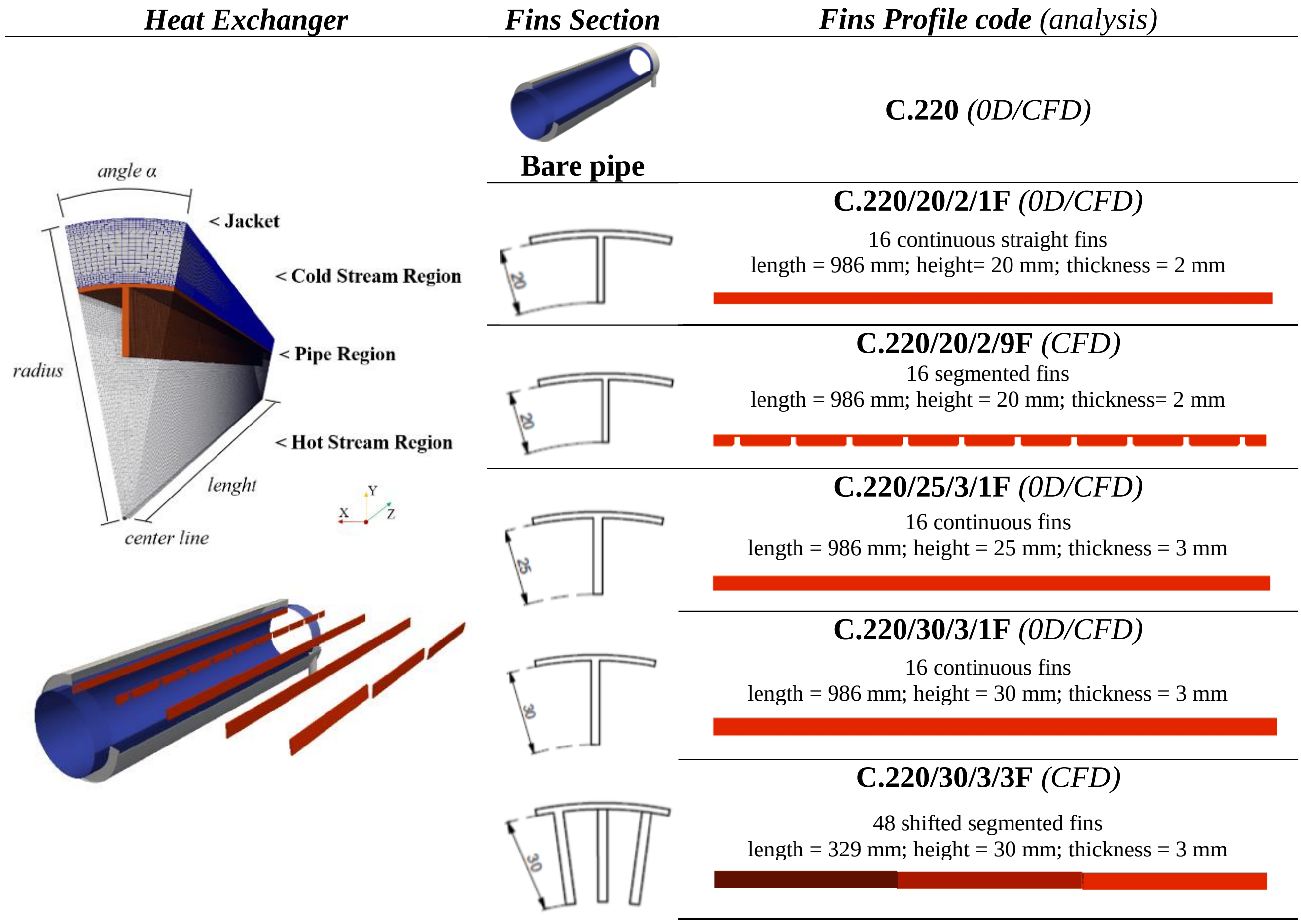

Heat Exchanger
Fins Section
Fins Profile code (analysis)
angle α
< Jacket
< Cold Stream Region
< Pipe Region
< Hot Stream Region
radius
lenght
center line
Y
X
Z
Bare pipe
C.220 (0D/CFD)
C.220/20/2/1F (0D/CFD)
16 continuous straight fins
length = 986 mm; height= 20 mm; thickness = 2 mm
20
C.220/20/2/9F (CFD)
16 segmented fins
length = 986 mm; height = 20 mm; thickness= 2 mm
20
C.220/25/3/1F (0D/CFD)
16 continuous fins
length = 986 mm; height = 25 mm; thickness = 3 mm
25
C.220/30/3/1F (0D/CFD)
16 continuous fins
length = 986 mm; height = 30 mm; thickness = 3 mm
30
C.220/30/3/3F (CFD)
48 shifted segmented fins
length = 329 mm; height = 30 mm; thickness = 3 mm
30

Figure 7

CFD Simulation results – Hot stream region

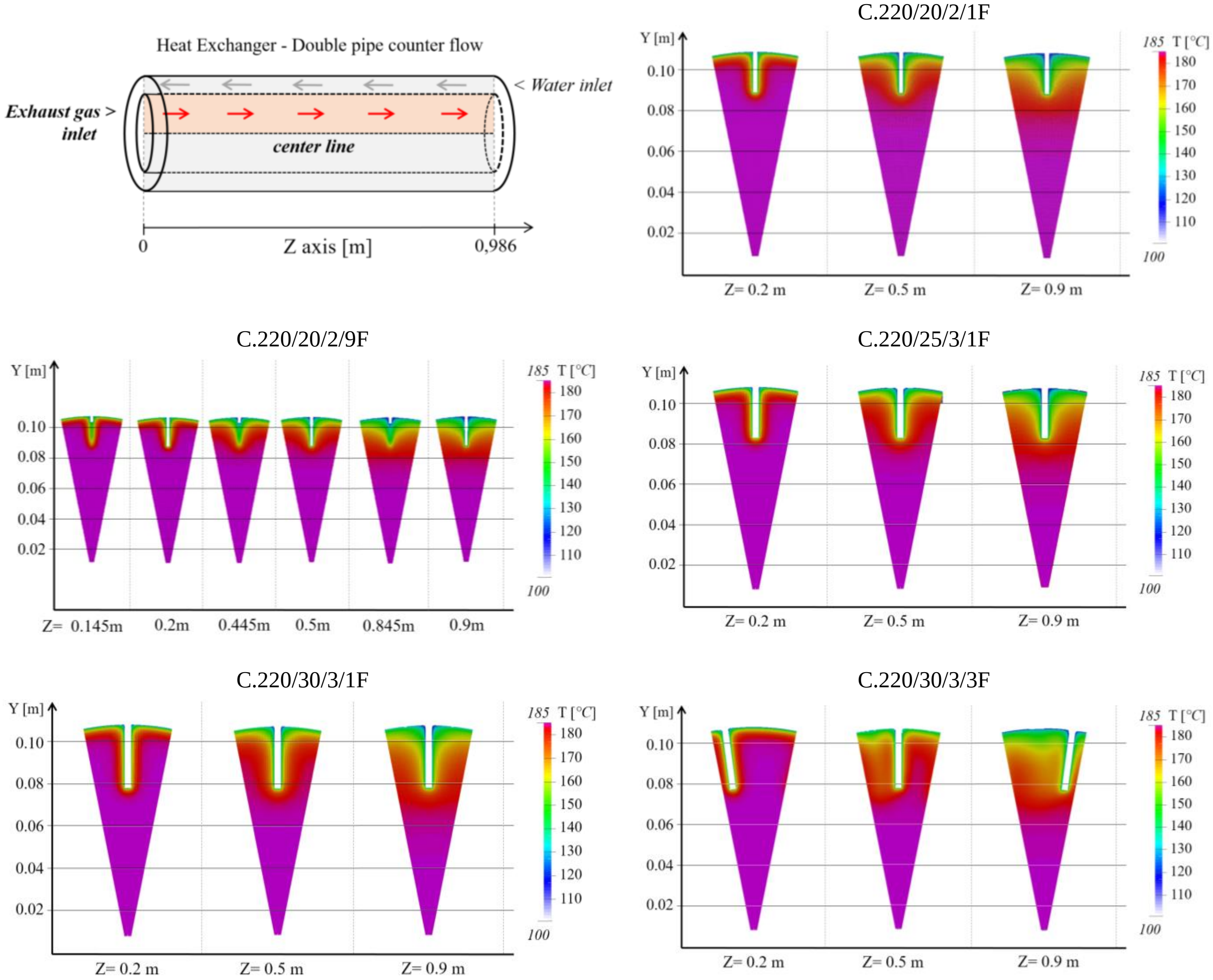

Figure 8

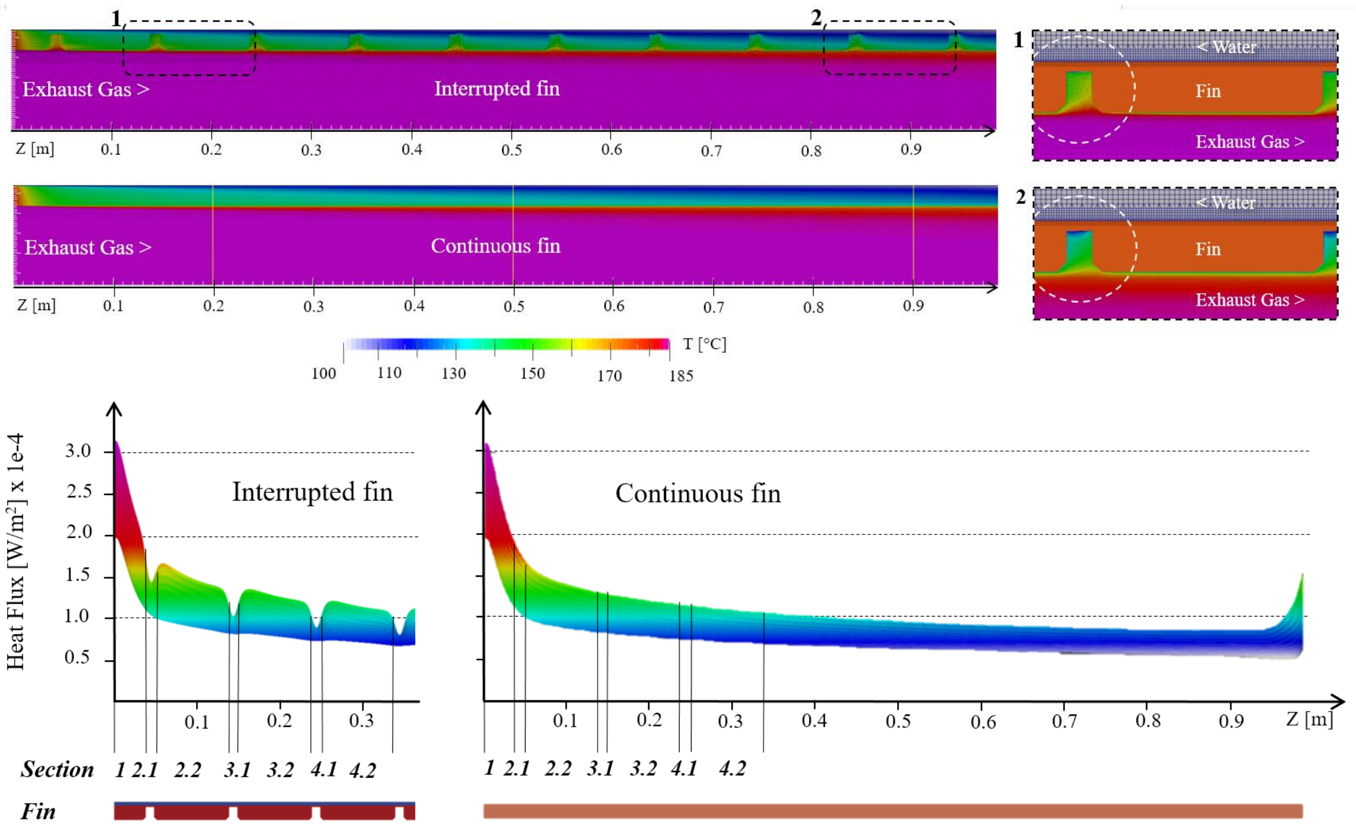

1
2
Exhaust Gas >
Interrupted fin
Z [m]
0.1
0.2
0.3
0.4
0.5
0.6
0.7
0.8
0.9
< Water
Fin
Exhaust Gas >
Continuous fin
T [°C]
100
110
130
150
170
185
Heat Flux [W/m^2] x 1e-4
3.0
2.5
2.0
1.5
1.0
0.5
Section
1 2.1 2.2 3.1 3.2 4.1 4.2
Fin

Figure 9

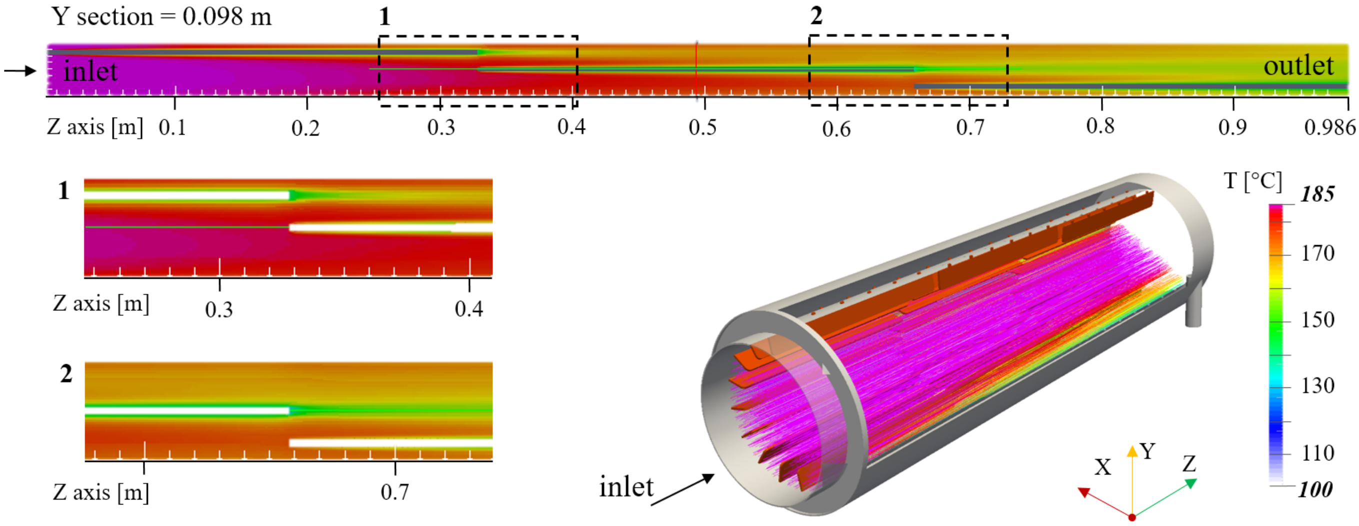
Y section = 0.098 m
1
2
inlet
outlet
Z axis [m] 0.1
0.2
0.3
0.4
0.5
0.6
0.7
0.8
0.9
0.986
1
Z axis [m]
0.3
0.4
2
Z axis [m]
0.7
inlet
T [°C]
185
170
150
130
110
100
X
Y
Z

Figure 10

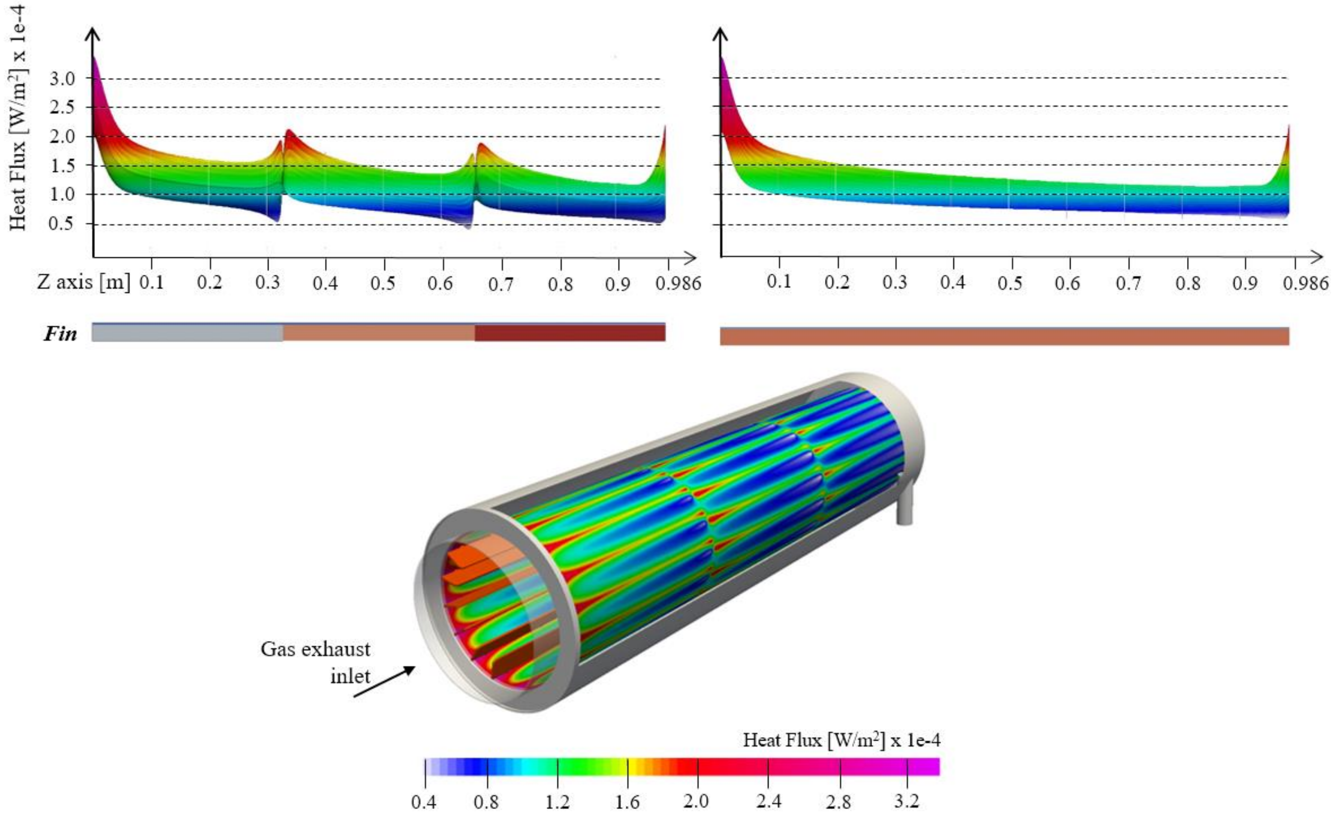
Heat Flux [W/m2] x 1e-4
3.0
2.5
2.0
1.5
1.0
0.5
Z axis [m] 0.1 0.2 0.3 0.4 0.5 0.6 0.7 0.8 0.9 0.986
0.1 0.2 0.3 0.4 0.5 0.6 0.7 0.8 0.9 0.986
Fin
Gas exhaust
inlet
Heat Flux [W/m2] x 1e-4
0.4 0.8 1.2 1.6 2.0 2.4 2.8 3.2

Figure 11

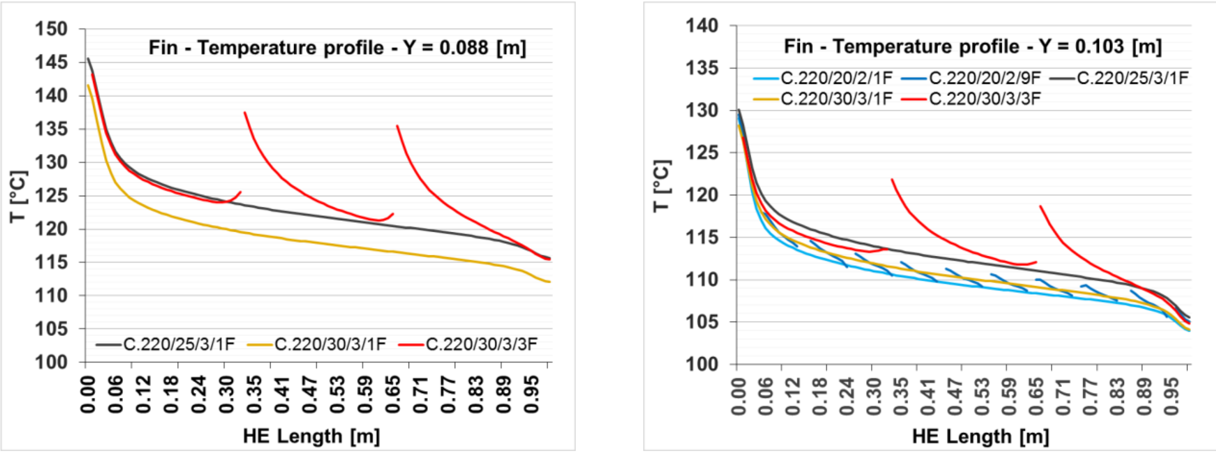
Fin - Temperature profile - Y = 0.088 [m]
T [°C]
HE Length [m]
C.220/25/3/1F
C.220/30/3/1F
C.220/30/3/3F
Fin - Temperature profile - Y = 0.103 [m]
C.220/20/2/1F
C.220/20/2/9F
C.220/25/3/1F
C.220/30/3/1F
C.220/30/3/3F
T [°C]
HE Length [m]

Figure 12

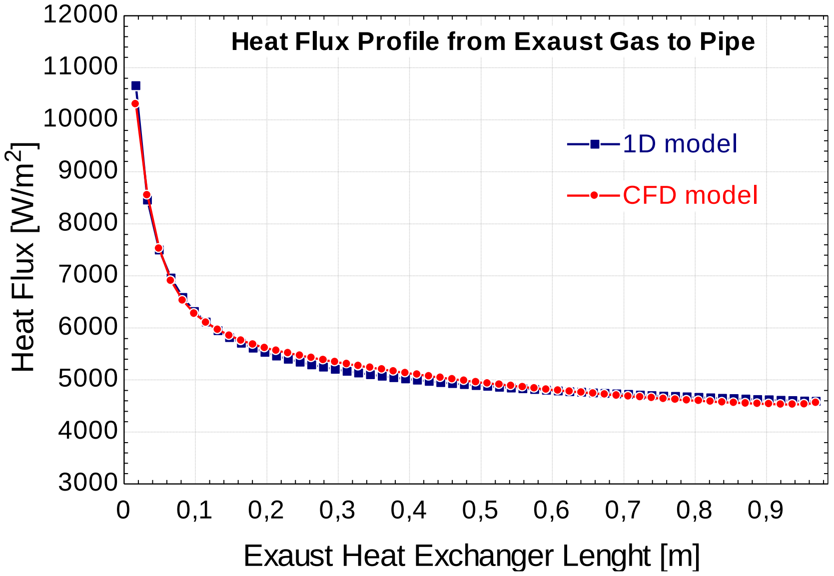
Heat Flux Profile from Exaust Gas to Pipe
Heat Flux [W/m2]
12000
11000
10000
9000
8000
7000
6000
5000
4000
3000
0
0,1
0,2
0,3
0,4
0,5
0,6
0,7
0,8
0,9
Exaust Heat Exchanger Lenght [m]
1D model
CFD model

Figure 13

a) Front view *b) Back view*

Figure 14

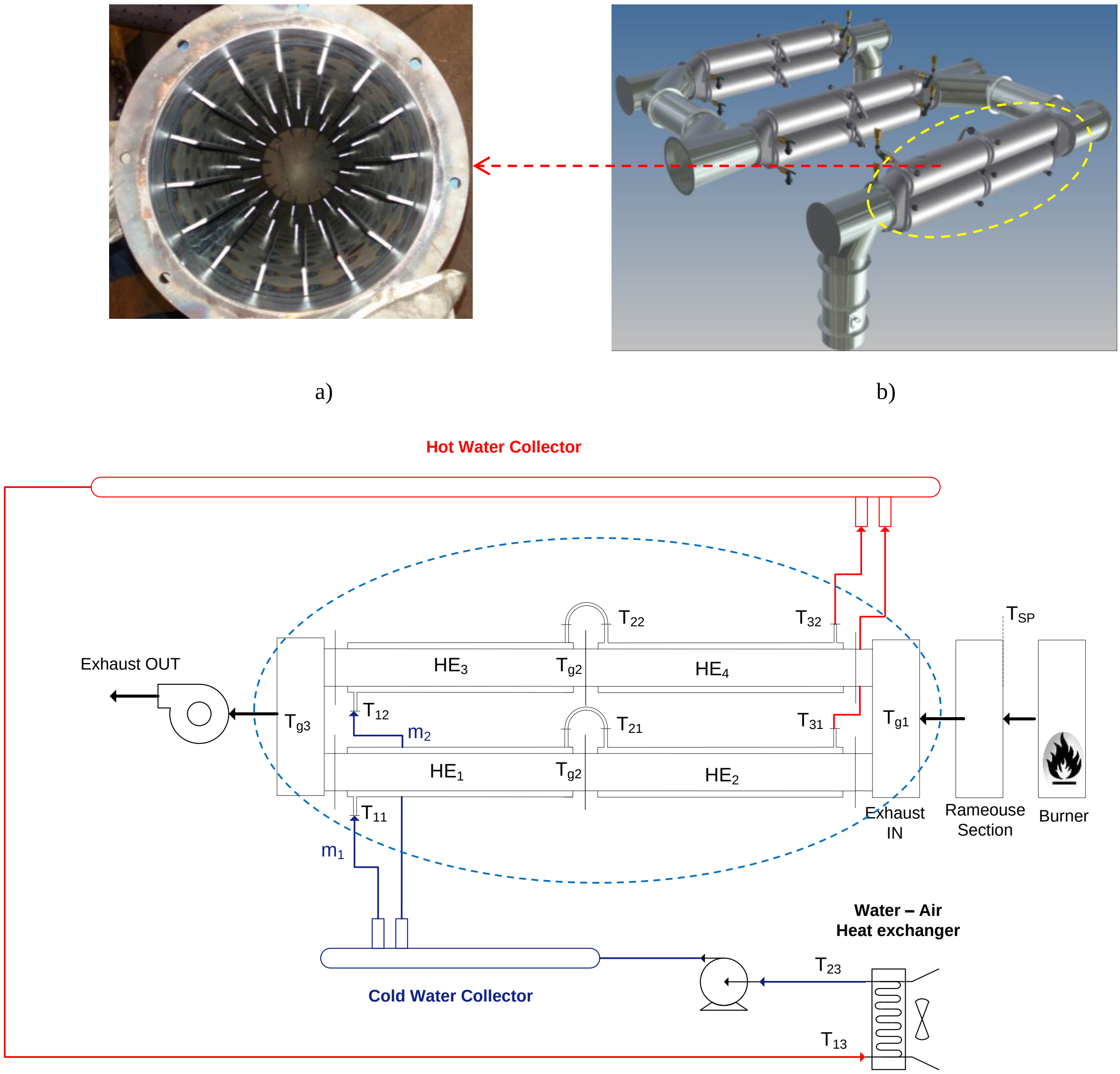

a) b)

c)

Figure 15

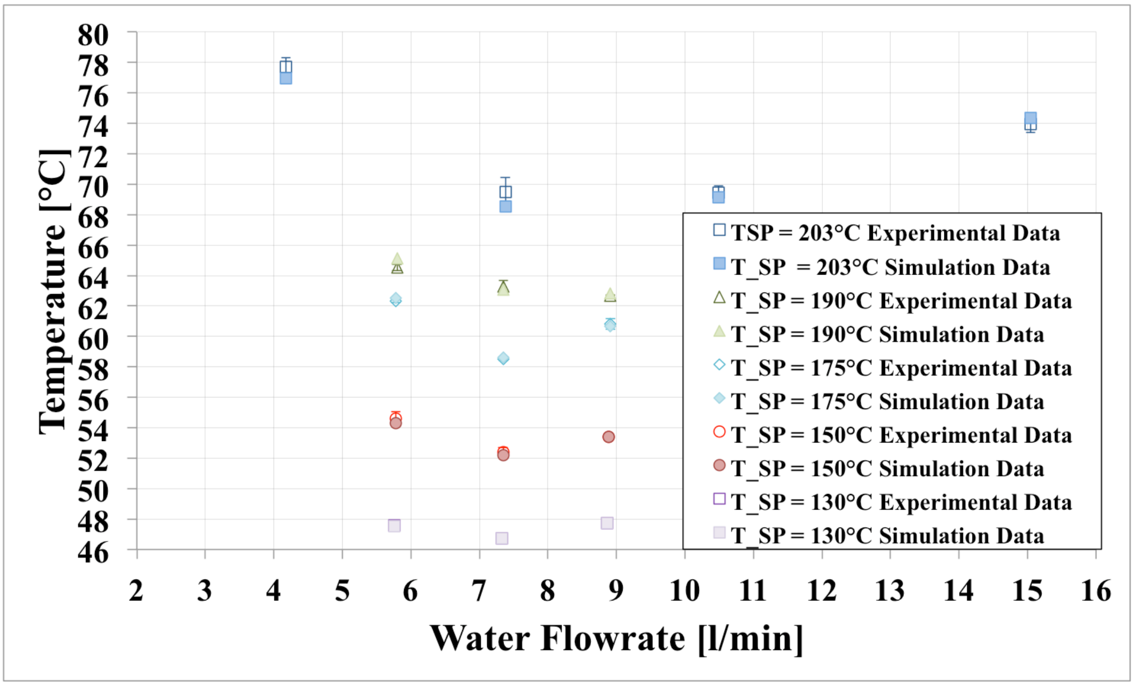
Temperature [°C]
80
78
76
74
72
70
68
66
64
62
60
58
56
54
52
50
48
46
2
3
4
5
6
7
8
9
10
11
12
13
14
15
16
Water Flowrate [l/min]
TSP = 203°C Experimental Data
T_SP = 203°C Simulation Data
T_SP = 190°C Experimental Data
T_SP = 190°C Simulation Data
T_SP = 175°C Experimental Data
T_SP = 175°C Simulation Data
T_SP = 150°C Experimental Data
T_SP = 150°C Simulation Data
T_SP = 130°C Experimental Data
T_SP = 130°C Simulation Data

Figure 16

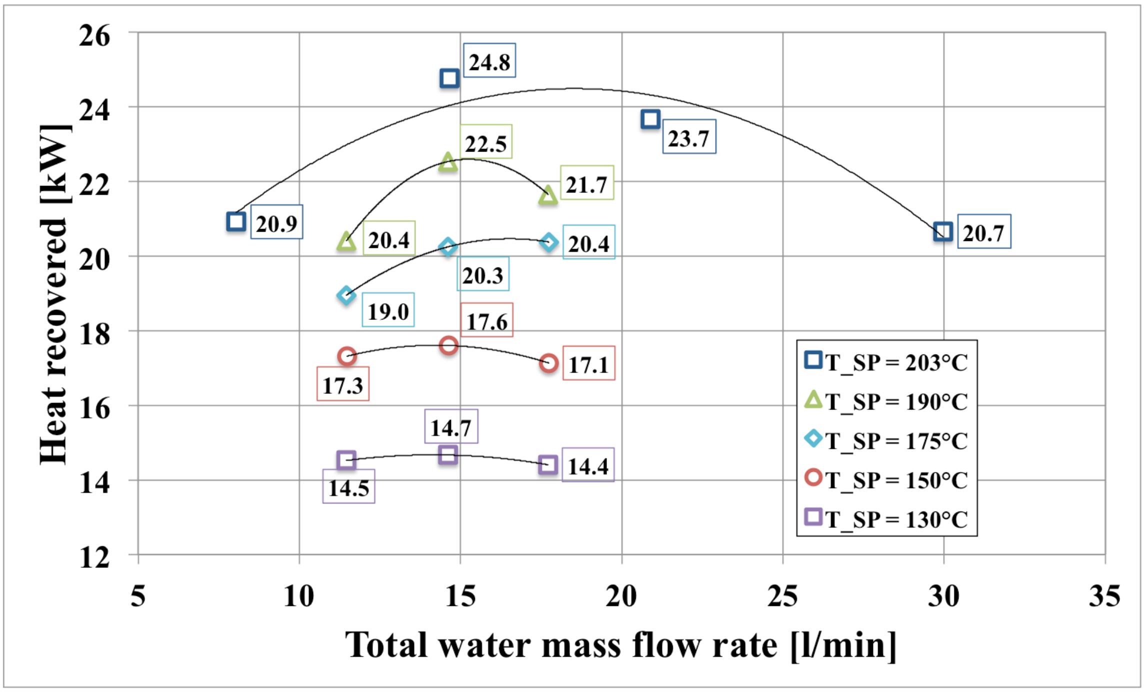
Heat recovered [kW]
Total water mass flow rate [l/min]
26
24
22
20
18
16
14
12
5
10
15
20
25
30
35
24.8
23.7
20.9
20.7
22.5
21.7
20.4
20.4
20.3
19.0
17.6
17.3
17.1
14.7
14.5
14.4
T_SP = 203°C
T_SP = 190°C
T_SP = 175°C
T_SP = 150°C
T_SP = 130°C

Figure 17

Tables

Colour Code Legend	**Datasheet inputs**	**Assumed inputs**	**Outputs from calculation model**
SYSTEM COMPONENTS	**Circuit Points [-]**	**Mass flowrate** m [kg/s]	**Temperature** [C]
WATER LOOP			
Pump – inlet	**1**	**1.36**	**95.2**
Pump – outlet	**2**	1.36	95.2
HE_1 gas/water output	**3**	1.36	96.9
HE_2 gas/ water output	**4**	1.36	98.4
HE_3 gas/ water output	**5**	1.36	**99.7**
EXHAUST GAS LINE			
Suction cell 2 $m_6 = 1/2\ m_{11}$	**6**	**1.60**	**185**
	7	1.60	179.4
	8	1.60	174.2
Suction cell 1 $m_9 = 1/2\ m_{11}$	**9**	**1.60**	**176**
	10	1.60	171.1
Exhausts Output	**11**	3.20	172.7
		9400 Sm^3/h	
MAKEUP AIR			
HE air/water Inlet	**12**	0.446	**31.8**
HE air/water Outlet	**13**	0.446	**88.3**
		1.316 Sm^3/h	

Table 1

HEAT EXCHANGERS PARAMETERS	**Power** [kW]	**Overall HT coefficient U_{tot}** [W/m^2K^{-1}]	**HE Surface area** [m^2]
EXHAUST GAS/WATER Hes			
HE1	9.118	20.84	2.539
HE2	8.385	20.83	2.539
HE3	7.895	20.84	2.539
AIR / WATER HE			
HE4	25.31	**41.0**	20.94
	Friction Power	**Exhaust gas velocity**	**LMTD**
	[W]	[m/s]	[K]
HE1	39.6	19.72	86.18
HE2	39.2	19.62	79.26
HE3	39	19.58	74.61
Comparative table: Model vs. Datasheet			
	Thermal power [kW]	**Volume flow rate [Sm^3/h]**	**HE surface area [m^2]**
Datasheet	25.29	1310	20.80
0D Model	25.31	1316	20.94

Table 2

Colour Code Legend		**Assumed inputs**	**Outputs from calculation model**
SYSTEM COMPONENTS	**Circuit Points**	**Mass flowrate**	**Temperature**
	[n°]	m [kg/s]	[C]
WATER LOOP			
Pump – inlet	**1**	**16**	**95.2**
Pump – outlet	**2 – 3.1-3.2-3.3**	16	95.2
HE_1 gas/water output	**4.1**	5.33	96.35
HE_2 gas/ water output	**4.2**	5.33	96.14
HE_3 gas/ water output	**4.3**	5.33	**96.23**
HE_4 air/water inlet	**5**	16	**96.24**
EXHAUST GAS LINE			
Suction cell 2 $m_6 = 1/2\ m_{11}$	**6**	**1.60**	**185**
	7	1.60	169.1
	8	1.60	156.1
Suction cell 1 $m_9 = 1/2\ m_{11}$	**9**	**1.60**	**176**
	10	1.60	161.7
Exhausts Output	**11**	3.20	158.9
		9400 Sm^3/h	
MAKEUP AIR			
HE air/water Inlet	**12**	0.575	**31.8**
HE air/water Outlet	**13**	0. 575	**88.3**
		3631 Sm^3/h	

Table 3

HEAT EXCHANGERS PARAMETERS	**Power** [kW]	**Overall HT coefficient U_{tot}** $[W/m^2K^{-1}]$	**HE Surface area** $[m^2]$	
EXHAUST GAS/WATER Hes			Bare pipe	Fins
HE1	25.79	57.05	2.726	1.893
HE2	21.17	49.08	2.726	1.893
HE3	23.17	49.17	2.726	1.893
AIR / WATER HE				
HE4	70.15	**41.0**	64.46	
	Friction Power	**Exhaust gas velocity**	**LMTD**	
	[W]	[m/s]	[K]	
HE1	183.8	25.89	81.11	
HE2	204.5	25.39	66.69	
HE3	208.1	25.6	72.94	
Comparative table: Bacis vs. Improved configuration				
	Thermal power [kW]	**Volume flow rate $[Sm^3/h]$**	**HE surface area $[m^2]$**	
Previous configuration	25.31	1316	20.94	
Improved configuration	70.13	3631	64.46	
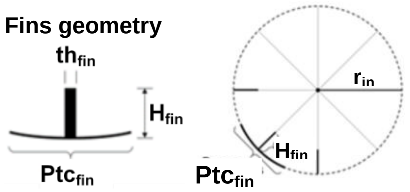	H_{fin} [m]	0.03		
	th_{fin} [m]	0.003		
	Ptc_{fin} [m]	0.042		

Table 4

<table>
<tr><th colspan="9">HEAT RECOVERY SYSTEM - 0D Analysis - Exhaust Gas Heat Exchangers Configurations</th><th></th></tr>
<tr><th></th><th colspan="5">Exhaust gas heat exchanger</th><th colspan="4">Finned inner pipe - Fins</th></tr>
<tr><th>Label</th><th>Inner diameter [mm]</th><th>Outer diameter [mm]</th><th>Inner jacket diameter [mm]</th><th>Length of jacket [mm]</th><th>Twin pipes conf.</th><th>Number [n°]</th><th>Height [mm]</th><th>Thick. [mm]</th><th>Height/pitch ratio λ_{fin}</th></tr>
<tr><td colspan="9">HEAT EXCHANGER - COURRENT TYPE "A"[(1)] WITH SERIES WATER CIRCUIT</td><td></td></tr>
<tr><td>A.350</td><td>350</td><td>354</td><td>410</td><td>2.283</td><td>-</td><td>-</td><td>-</td><td>-</td><td></td></tr>
<tr><td colspan="9">HEAT EXCHANGER - NEW TYPE "C"[(2)]WITH PARALLEL WATER CIRCUIT</td><td></td></tr>
<tr><td>C.350</td><td>350</td><td>354</td><td>410</td><td>2.283</td><td>-</td><td>-</td><td>-</td><td>-</td><td></td></tr>
<tr><td>C.250</td><td rowspan="2">246</td><td rowspan="2">250</td><td rowspan="2">308</td><td rowspan="2">2 x 986</td><td>x</td><td>-</td><td>-</td><td>-</td><td></td></tr>
<tr><td>C.250/F</td><td>x</td><td>8 / 12 / 16</td><td>20</td><td>2</td><td>0.208/0.31/0.42</td></tr>
<tr><td>C.220</td><td rowspan="2">216</td><td rowspan="2">220</td><td rowspan="2">278</td><td rowspan="2">2 x 986</td><td>x</td><td>-</td><td>-</td><td>-</td><td></td></tr>
<tr><td>C.220/F</td><td>x</td><td>8 / 12 / 16</td><td>20</td><td>2</td><td>0.234/0.35/0.47</td></tr>
<tr><td>C.200</td><td rowspan="2">196</td><td rowspan="2">200</td><td rowspan="2">258</td><td rowspan="2">2 x 986</td><td>x</td><td>-</td><td>-</td><td>-</td><td></td></tr>
<tr><td>C.200/F</td><td>x</td><td>8 / 12 / 16</td><td>20</td><td>2</td><td>0.26/0.39</td></tr>
</table>

(1) Co-current bare pipe - Water loop with heat exchangers in series

(2) New twin-can exhaust gas pipe - Water loop with manifold distribution to exhaust heat exchangers

Table 5

<table>
<tr><th colspan="8">Domain</th></tr>
<tr><td>Lenght</td><td colspan="2">Radius</td><td colspan="3">Angle α</td><td colspan="2">Mesh</td></tr>
<tr><td>0,986 m</td><td colspan="2">0,138 m</td><td colspan="3">22,5°</td><td colspan="2">Structured Grid</td></tr>
<tr><td colspan="8">Simulation parameters</td></tr>
<tr><td>CFD Code</td><td colspan="2">Simulation type</td><td colspan="3">Solver</td><td colspan="2">Turbulence model</td></tr>
<tr><td>OpenFOAM</td><td colspan="2">Stationary</td><td colspan="3">chtMultiRegionSimpleFoam</td><td colspan="2">K-Omega SST</td></tr>
<tr><td colspan="3">Hot Stream Region inlet - Exhaust gas</td><td colspan="5">Cold Stream Region inlet - Water</td></tr>
<tr><td>Temperature</td><td colspan="2">Velocity</td><td colspan="3">Temperature</td><td colspan="2">Velocity</td></tr>
<tr><td>185°C</td><td colspan="2">25,89 m/s</td><td colspan="3">95,2°C</td><td colspan="2">0,1271 m/s</td></tr>
<tr><td colspan="8">Grid resolution</td></tr>
<tr><td>Heat Exchanges ID</td><td>C.220/20/2/1F</td><td colspan="2">C.220/20/2/9F</td><td>C.220/25/3/1F</td><td colspan="2">C.220/30/3/1F</td><td>C.220/30/3/3F</td></tr>
<tr><td>Cells numbers</td><td>3.074.269</td><td colspan="2">3.074.176</td><td>3.708.853</td><td colspan="2">3.984.234</td><td>5.037.362</td></tr>
</table>

Table 6

CFD Model	**C.220/20/2/1F**		**C.220/20/2/9F**		**Heat flux Ratio relative difference [%]**
Section [n°]	fin height [m]	Heat flux [W]	fin height [m]	Heat flux [W]	C.220/20/2/1F / C.220/20/2/9F [%]
1	0.02	30.31	0.02	30.28	0.1
2.1	0.02	5.65	0.004	5.28	7.0
2.2	0.02	42.33	0.02	42.54	-0.5
3.1	0.02	4.28	0.004	3.95	8.3
3.2	0.02	36.32	0.02	36.43	-0.3
4.1	0.02	3.83	0.004	3.49	9.6
4.2	0.02	33.04	0.02	32.90	0.4

Table 7

HEAT RECOVERY SYSTEM - 0D/CFD Comparative Analysis - Results					
Heat exchanger		**0D Analysis**		**CFD Analysis**	
		Heat recovery [kWt]	Relative increase to the bare pipe [%]	Heat recovery [kWt]	Relative increase to the bare pipe [%]
Label	Id				
C.220	bare pipes	3,75	-	3,65	-
C.220/F	C.220/20/2/1F	5,75	53,1%	5,66	55,1%
	C.220/20/2/9F	-	-	5,60	53,4%
	C.220/25/3/1F	6,23	65,9%	6,30	72,6%
	C.220/30/3/1F	6,60	75,7%	6,78	85,8%
	C.220/30/3/3F	-	-	7,20	97,3%

Table 8

T_{SP} [°C]	Branch Mass flow rate [l/min]	Heat Recovered [kW] Simulation Data	Heat Recovered [kW] Experimental Data	Standard Deviation of experimental data [kW]
203	4.17	4.56	4.81	± 0.15
	7.38	4.72	5.21	± 0.12
	10.49	4.65	4.87	± 0.10
	15.04	4.40	3.98	± 0.07
190	5.80	4.56	4.34	± 0.10
	7.35	4.60	4.71	± 0.07
	8.91	4.56	4.48	± 0.08
175	5.78	4.16	4.09	± 0.04
	7.35	4.26	4.24	± 0.04
	8.91	4.15	4.24	± 0.05
150	5.78	3.59	3.74	± 0.04
	7.34	3.62	3.72	± 0.06
	8.89	3.55	3.55	± 0.04
130	5.76	3.10	3.14	± 0.03
	7.33	3.08	3.08	± 0.04
	8.87	3.01	2.99	± 0.04

Table 9